J Polym Res (2015) 22: 156
DOI 10.1007/s10965-015-0799-y

ORIGINAL PAPER

Magnetic graphene oxide mesoporous silica hybrid nanoparticles with dendritic pH sensitive moieties coated by PEGylated alginate-*co*-poly (acrylic acid) for targeted and controlled drug delivery purposes

Ali Pourjavadi[1] · **Alireza Shakerpoor**[1] · **Zahra Mazaheri Tehrani**[1] · **Ali Bumajdad**[2]

Received: 10 March 2015 / Accepted: 10 July 2015 / Published online: 21 July 2015

Abstract In this study synthesis of a drug delivery system (DDS) is described which has several merits over its counterparts. In order to synthesize this nano-carrier, graphene oxide nano-sheets are used to accommodate MCM-41 nanoparticles. Furthermore Fe_3O_4 nanoparticles are introduced to this nano-material to produce a traceable nanoparticle. Since cancerous tissues have lower pH than healthy tissues, pH-sensitive oligomers are attached to this nano-material. Finally the nano-carrier is wrapped by a biocompatible shell (PEGylated sodium alginate); this polymeric shell makes the DDS capable of a more controllable drug release. By measuring in vitro situation, 'loading content%' and 'entrapment efficiency%' proves to be 21 and 93.5 % respectively. In an acidic medium, the drug carrier without a polymeric shell (naked DDS) releases the whole of its drug content in 18 h, while the drug carrier with a polymeric shell (core-shell DDS) releases 45 % of its drug content during 48 h.

Keywords Drug delivery systems · Stimuli-sensitive polymers · pH-sensitive nanoparticles · PEGylated sodium alginate · MCM-41 mesoporous silica

Introduction

Current medical treatments have helped many cancerous patients to overcome their disease by employing various anticancer drugs. Though promising and practical, therapeutic agents and anticancer drugs suffer from some drawbacks: usually they do not spot cancerous tissue precisely and harm its surrounding sound tissues as well [1]. Furthermore some anticancer drugs have low therapeutic indices that cause higher concentrations of them to be employed which in turn brings about resistance against these pharmaceuticals; accordingly in a vicious cycle each time a higher concentration of drug should be utilized. Finding less invasive and less frequent drug intake methods have been the subject of interests for many researchers who are working in this area. Smart drug carriers, such as: polymeric nanoparticles (NPs), polymeric micells, dendrimers, liposomes, carbon nanotubes and so on, are considered as complementary solutions which amend and improve the action of anticancer drugs [2]. Among these carrier systems, NPs are better off compared to others due to their dramatic higher immuno-compatibility and biocompatibility [2]. Also these drug carriers could be tailor-made for a specific kind of drug or an especial tissue or cell.

Due to their high rate of metabolism, cancerous cells usually metabolize glucose partially and transform it into lactic acid, which gives rise to an acidic medium [3]. This feature is a helpful mean for a passive targeting of cancer cells by adding some pH-sensitive moieties. All pH-sensitive moieties contain pendant acidic or basic groups that either accept or donate protons in response to the environmental pH [4]. The pH-sensitive polymer may be linear, grafted, a copolymer or a hydrogel. Several pH-sensitive moieties have been reported such as: CS/PVP (chitosan/polyvinyl pyrrolidone), spherical crosslinked beads using chitosan, glycine and glutaraldehyde and other cationic hydrogels [5, 6]. However we introduced an amine oligomer (pentaethylene hexamine) because the safest graphene derivative in biocompatibility respect is G-NH_2 [7]. Finally the core of the drug carrier was encompassed by a polymeric shell which was stabilized on the core by

✉ Ali Pourjavadi
purjavad@sharif.edu

[1] Polymer Laboratory, Chemistry Department, Sharif University of Technology, P.O. Box 11155-8639, Tehran, Iran

[2] Department of Chemistry, Faculty of Science, Kuwait University, P.O. Box 5969, Safat 13060, Kuwait

Table 1 Porous structure of some broadly used mesoporous materials [11, 12]

Mesoporous solid	Space group	Pore diameter (nm)	Structure
MCM-41	P6mm	2–5	Hexagonal 1D channel
MCM-48	Ia3d	2–5	Bicontinuous 3D
SBA-15	P6mm	5–10	Hexagonal 1D channel
SBA-16	Im3m	Min 1–6; Max 4–9	Body center arrangement
SBA-1	Pm3n	2–4	Cubic 3D
SBA-3	P6mm	2–4	2D hexagonal
MSU	P6mm	2–5	2D hexagonal
HMS	P6mm	2–5	Hexagonal

electrostatic interactions such as hydrogen bond. The reason behind introducing a polymeric shell lies in two facts: first a polymeric shell leads to a more controllable drug release from the drug carrier and it prevents the drug from being released at once (which is proved by results of this research). Second this polymeric shell allows for introducing biocompatible and immunocompatible moieties like poly ethylene glycol (PEG) groups which in turn prolong the NP circulation in the blood stream by repelling protein adsorption onto the NP [2]. In synthesizing this core-shell DDS three kinds of NPs were employed; different aspects of these NPs are discussed in the following sections.

GO nano-sheets

Graphite which is constituted of numerous single atomic layers of sp [2] carbon atoms stacked on each other could be transformed into its single layer constituents called graphene, either by mechanical exfoliation ('Scotch-tape' method) or by chemical oxidation ('Hummers' method). The latter process oxidizes the graphene layers and produces graphene oxide (GO) nano-sheets. These nano-sheets have unique characteristics which make them appropriate for various applications ranging from nanoelectronics and quantum physics to catalysis and medicine. The properties of graphene nanomaterials which are crucial for drug delivery applications comprise surface area, number of layers, lateral dimension, surface chemistry and purity [8]. The surface area of GO (2600 m^2/g) is four times greater than any other nanomaterial utilized for drug delivery [9]. Furthermore it has been proved that GO can be regarded as a relatively safe material at the mammalian cellular level [6]. Nonetheless the understanding of accurate uptake mechanism and toxicity of graphene-based materials require extra investigations.

Mesoporous nanoparticles

As the 1990s was unfolded some highly ordered silica materials were discovered. Owe to their stable structure and well-defined surface properties, mesoporous materials seem ideal choices for encapsulation, transferring and storing pharmaceutical drugs. Table 1 presents the porous structure of some mesoporous materials which have been utilized for drug delivery purposes. The wall of these mesoporous materials is constituted of an entangled network of siloxane bridges and free silanol groups which can act as reacting hubs for appropriate guest functional groups as well as acting as proper matrices for dynamic and continuous adsorption and desorption of pharmaceuticals [10].

In this work, we used doxorubicin as an anticancer drug examined for drug delivery purpose and MCM-41 as the appropriate mesoporous material that accommodated these organic molecules.

Iron magnetic nanoparticles (MNPs)

Due to their low toxicity, iron oxide materials have been constantly considered for biomedical applications. Among different types of iron oxide materials (Table 2), magnetite and maghemite seem great options for drug delivery purposes. They solve the problem associated with the nonspecific attack of anticancer drugs against both healthy and cancerous cells; magnetized DDSs could be tracked and guided by an exterior magnetic field. Furthermore MNPs are considered as labeling agents as well as contrast agents for magnetic resonance imaging. Recently Calero et al. have confirmed the high cell labeling efficiency and very low toxicity of different coated MNPs into HeLa cells [13].

Table 2 Various types of iron oxide materials [14]

Mineral name	Structure	Density (g cm^{-3})	Type of magnetism	Color
Goethite (α-FeOOH)	Orthorhombic	4.26	Antiferromagnetic	Yellow-brown
Hematite (α-Fe_2O_3)	Rhombohedral hexagonal	5.26	Weakly ferromagnetic	Red
Magnetite (Fe_3O_4)	Cubic	5.18	Ferrimagnetic	Black
Maghemite (Υ-Fe_2O_3)	Cubic or tetragonal	4.87	Ferrimagnetic	Reddish-brown

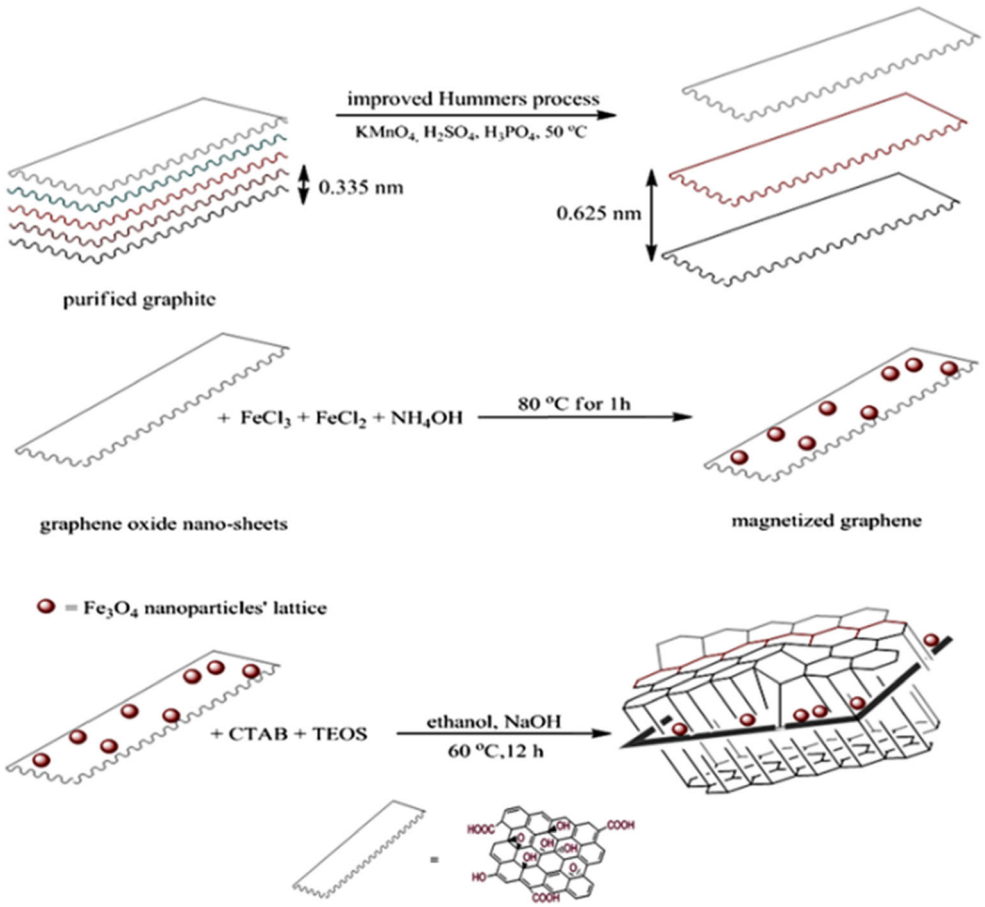

Fig. 1 Preparation of magnetic double-sided mesoporous graphene oxide

In this research, we designed an anticancer drug nanocarrier with pH-sensitive behavior. The magnetic mesoporous silica nanoparticles which were modified by dendritic pentaethylene hexamine were used as pH-sensitive core of the drug carrier. They were wrapped by PEGylated sodium alginate as the pH-sensitive shell. As an anticancer drug,

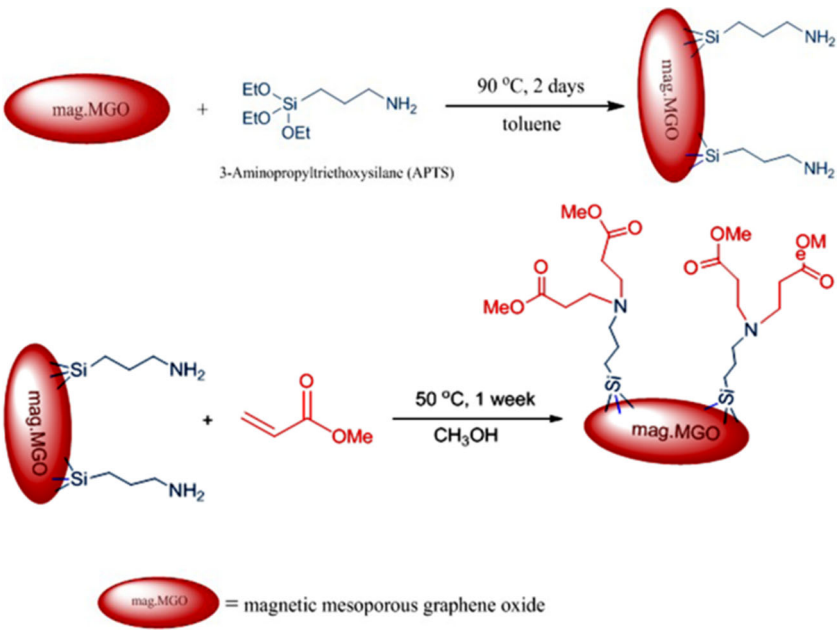

Fig. 2 Methyl acrylate functionalized nanoparticles

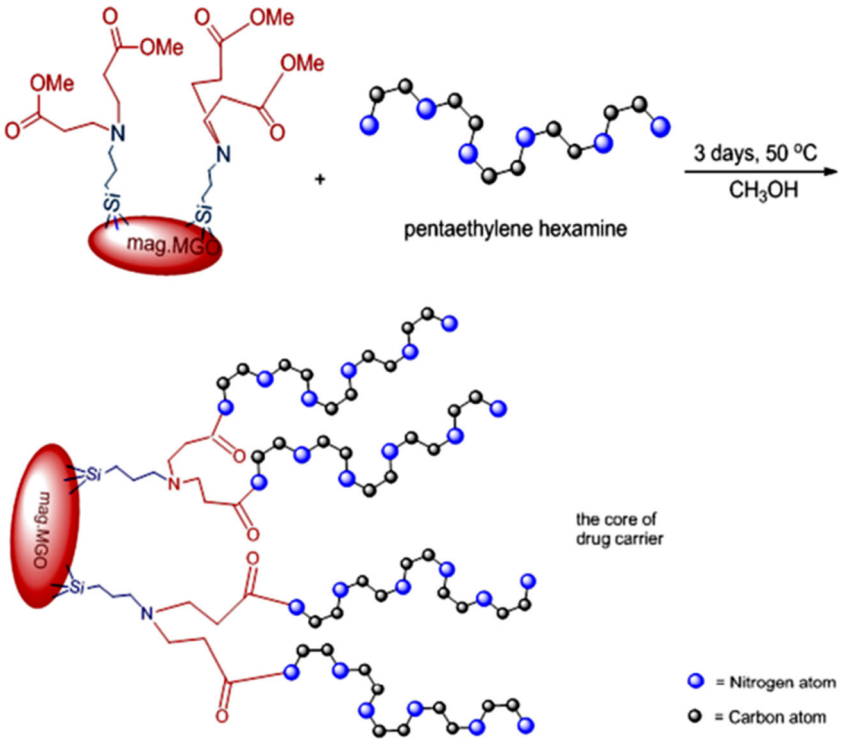

Fig. 3 pH-sensitive amine oligomers grafted on the nanoparticles

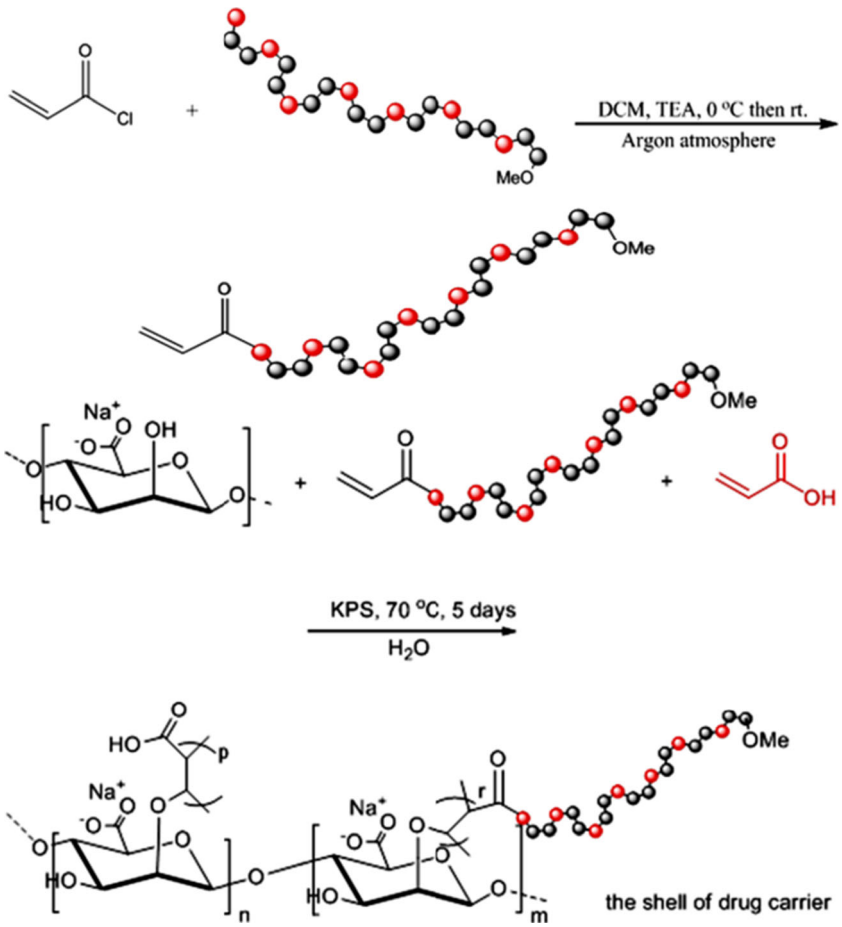

Fig. 4 Synthetic route of polymeric shell

doxorubicin was loaded on the core of the nanocarrier and the in vitro drug release was studied.

Experimental section

Materials

Natural graphite powder, sodium hydroxide, concentrated sulfuric acid, phosphoric acid, potassium permanganate, hydrogen peroxide (H_2O_2 30 %), ammonium hydroxide (NH_4OH 30 %), ferric chloride hexahydrate ($FeCl_3.6H_2O$ 98 %), ferrous chloride tetrahydrate ($FeCl_2.4H_2O$ 98 %), tetraethyl *ortho*silicate (TEOS), cetyl trimethylammonium bromide (CTAB), ammonium nitrate (NH_4NO_3), (3-Aminopropyl)triethoxysilane (APTS). Analytically pure methyl acrylate was purchased from East of China Chemical Corporation. Pentaethylene hexamine, poly (ethylene glycol) methyl ether 500 (mPEG 500) and acryloyl chloride were purchased from Alfa Aesar. Triethylamine (TEA), dried dichloromethane (DCM) and dried diethyl ether were provided from Merck. Sodium alginate was provided from Sigma-Aldrich, acrylic acid (AA) as ionic monomer distilled before use and potassium persulfate (KPS) as initiator, were provided from Merck. Doxorubicin hydrochloride (DOX) was obtained from India. Dialysis bag (M_n cutoff 12 KDa) was provided from Sigma. Phosphate buffer saline (PBS, pH 7.4 and 5.5) and all other materials were chemical grade and used as received.

Characterization techniques

'ABB Bomem MB-100' Fourier-transform infrared (FT-IR) spectrometer was used to confirm the structure of some intermediate and final synthesized species; KBr was utilized in making pellets. In vitro drug liberation was measured by 'Perkin-Elmer Lambda 25' UV–Vis spectrophotometer. Size distribution of nanoparticles was specified by 'Malvern 4700' DLS instrument at 298 K and deionized water as dispersant. Zeta (ζ) potential was measured by 'Zetasizer ZS Malvern' instruments. The morphology of nanoparticles was determined by 'Philips, Natick, MA, XL30' scanning electron microscope (SEM); a thin gold film was precipitated on the nanoparticles in advance. Specific surface areas, total pore volume and diameter were determined by 'Belsorp mini IIfrom BEL Japan' BET analyzer at 77 K and Nitrogen as adsorbate. Transmission electron microscopy (TEM) images were taken by a "JEOL's jem-1200 EXII" microscope. The wide angle X-ray diffraction patterns were recorded by a 'D5000 (Siemens)' XRD apparatus. The atomic force microscopy (AFM) images were recorded by 'veeco' Auto-probe cp-research microscope. CHN elemental analysis was done by 'Costech ECS 4010' elemental analyzer. Energy-dispersive X-ray (EDX) analysis was used for determination of elemental intensity and quality. Thermogravimetric analysis (TGA) was used to calculate the polymeric content of the DDS.

Table 3 The elemental (C, H and N) analysis results

	H%	C%	N%
GO	3.07	45.70	−1.0363
Fe_3O_4@GO	0.895	9.35	−1.2063

Synthesis of the core of DDS

Synthesis of the core of DDS includes three steps. Starting from pristine graphite, improved Hummers' method is employed to transform it into GO [15, 16]. Then magnetized GO (mag.GO) is transformed into magnetic double-sided mesoporous graphene oxide (mag.MGO) (Fig. 1) [17, 18].

This synthesis was accomplished in three main steps as depicted in the Figs. 1, 2, and 3.

The synthesis of graphene oxide

First pristine graphite should be converted into graphene oxide (GO). Since the conventional Hummers' method produces poisonous gases such as NO_2 and N_2O_4, we replaced it with the improved Hummers' method which produces more oxidized graphene sheets and preserves the intact planar structure of the graphite sheets as well. Based on our experience, the latter method (the improved Hummers' method) was highly exothermic and explosive, so the order of the introducing the

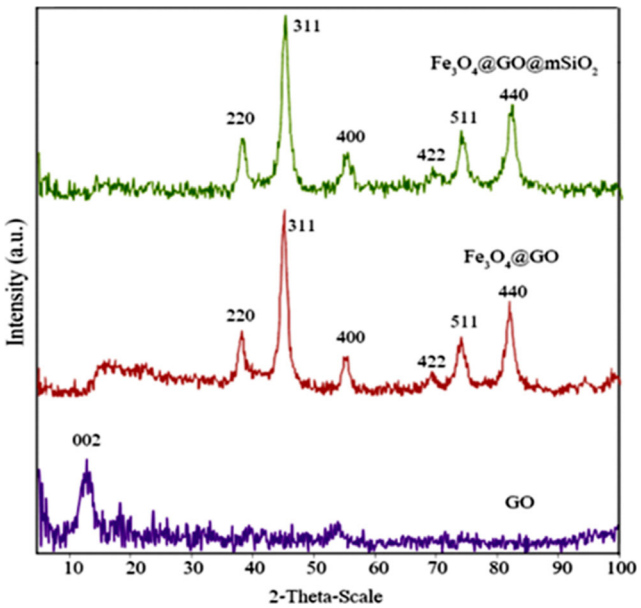

Fig. 5 X-ray diffraction patterns of GO, Fe_3O_4@GO and Fe_3O_4@$mSiO_2$@GO nanoparticles

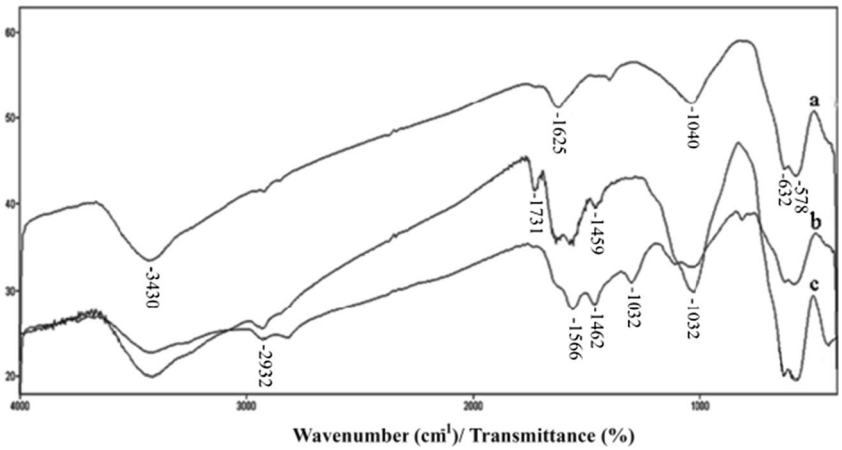

Fig. 6 FT-IR spectra of **a** Fe_3O_4@$mSiO_2$@GO nanoparticles, **b** Fe_3O_4@$mSiO_2$@GO/hexamine nanoparticles and **c** Fe_3O_4@$mSiO_2$@GO/acrylate

reagents to graphite was altered so that it became a safer method: the graphite powder (1 g) was combined with a 1:9 solution of H_3PO_4:H_2SO_4 (13:120 mL). While stirring this solution, $KMnO_4$ (6 g) was added gently to it during 3 h and at ambient temperature. The reaction was completed after stirring for 12 h at 50 °C. During the reaction the dark green oxidizing agents (Mn_2O_7) which is produced from dehydration of $KMNO_4$ by concentrated sulfuric acid was detectable. In the next step, the reaction's flask is submerged in an ice cooling bath and its solution is diluted by adding water (150 mL). H_2O_2 solution (30 %, 1 mL) is added gently into the reaction's flask to reduce the insoluble MnO_2 particles into soluble ions (in order to prevent them from being entrapped inside the graphene structure). During this reaction oxygen gas is released from the solution. The final product (GO) is precipitated by centrifuging the solution (6000 rpm for 10 min). Then it is washed by HCl solution (30 %, 3 times) and water (2 times). This precipitation is dried at 40 °C for 48 h.

The synthesis of magnetized GO (mag.GO)

The GO powder is added into a flask containing $FeCl_3.6H_2O$ (1.6 g) and $FeCl_2.4H_2O$ (0.6 g) and water as a dispersant (150 mL). This mixture is ultrasonicated for 30 min and then is added dropwise into another three necked flask which contains ammonia (NH_4OH 30 %, 25 mL) under N_2 atmosphere. This solution is stirred mechanically for 30 min at ambient temperature and then is stirred at 80 °C for 1 more h. The black precipitation is collected by a magnet and is washed by ethanol and water. Finally it is dried at 50 °C for 6 h.

The synthesis of double-sided mesoporous graphene oxide (mag.MGO)

For this synthesis, magnetized GO (mag.GO) (50 mg) is blended with CTAB (cetyl trimethylammonium bromide) (500 mg) and water (50 mL) and is ultrasonicated for 30 min. Then NaOH solution (0.01 M, 50 mL) and water (400 mL) is added to this mixture and is ultrasonicated for another 10 min. The reaction flask is heated for 30 min at 60 °C. Then under mechanical stirring, a 1:4 solution of TEOS:ethanol is added dropwise to the reaction's flask. This reaction is continued for 12 h at 60 °C. The final product is collected by magnet and is washed by water. The precipitation is dried at 40 °C for 6 h. There are entrapped CTAB nano-rods inside the MCM-41's pores which should be removed just before the drug loading. CTAB removing has been described in subsequent section.

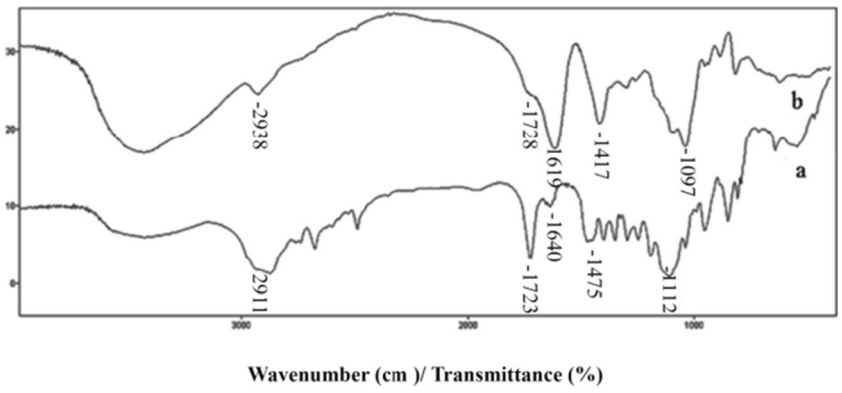

Fig. 7 FT-IR spectra of **a** mPEG-acrylate and **b** mPEG-acrylate-*g*-(alginate-co-poly acrylic acid)

Afterwards, magnetic Mesoporous GO (mag.MGO) (1 g) is ultrasonicated in toluene (40 mL) for 10 min. APTS (10 mL) is added to this solution and is refluxed at 80–90 °C for 24 h. The final product is collected by magnet, and is washed by ethanol. The precipitation is desiccated at 40 °C for 3 h. In the second step, the dried product (1 g) is ultrasonicated in methanol (100 mL) for 10 min and then methyl acrylate (20 g) is added to this solution. The solution is refluxed at 50 °C for 1 week to accomplish the Michael addition. The final product is collected by magnet and is washed by methanol. The precipitation is dried at 40 °C for 3 h (Fig. 2).

In the final step, the pH-sensitive amine oligomer is attached to the core of the drug carrier. To fulfill this, the synthesized product (0.4 g) in the previous step is ultrasonicated in methanol (30 mL) for 10 min and then pentaethylene hexamine (10 mL) is added to this solution (excessive amounts of pentaethylene hexamine are used for prevention of secondary amines' reaction with substrate). The solution is refluxed at 60 °C for 3 days. The final product is separated by a magnet and is washed by methanol. The precipitation is desiccated at 40 °C for 3 h (Fig. 3).

Synthesis of polymeric shell

As Fig. 4 demonstrates, synthesis of polymeric shell is accomplished in two stages. In the first stage mPEG (M_W=550) (2.25 g) is dissolved in DCM (25 mL) and then TEA (1.01 g) is added to this solution. Argon gas is bubbled in the solution for 5 min to purge it from oxygen molecules. Then the two-necked reaction's flask is submerged in an ice cooling bath and under argon atmosphere and magnetic stirring, acryloyl chloride (1.0 g) is added dropwise. After 3 h remaining in this condition, the reaction is continued in room temperature for 5 days. The final product (mPEG-acrylate) is precipitated in diethyl ether and is dried in vacuum. In the second stage, synthesis of the polymeric shell is completed. To achieve this, sodium alginate (0.5 g) is dissolved in hot water (25 mL) and then KPS (8 mg) is added into it. This solution is heated at 70–80 °C for 30 min. Afterwards mPEG-acrylate (0.7 g) is dissolved in water (25 mL) and is added into the reaction's flask. Then acrylic acid (0.3 g) is added gently into the flask. The reaction is continued for 5 days at 70–80 °C. The final product is precipitated in acetone and is dried at 40 °C for 48 h.

Drug loading and wrapping the core of DDS by polymeric shell

To impose the drug load on DDS, first CTAB nano-rods should be removed out of MCM-41 NPs. For this purpose, the synthesized core (1 g) and ammonium nitrate (0.15 g) are dissolved in methanol (15 mL). This solution is refluxed at

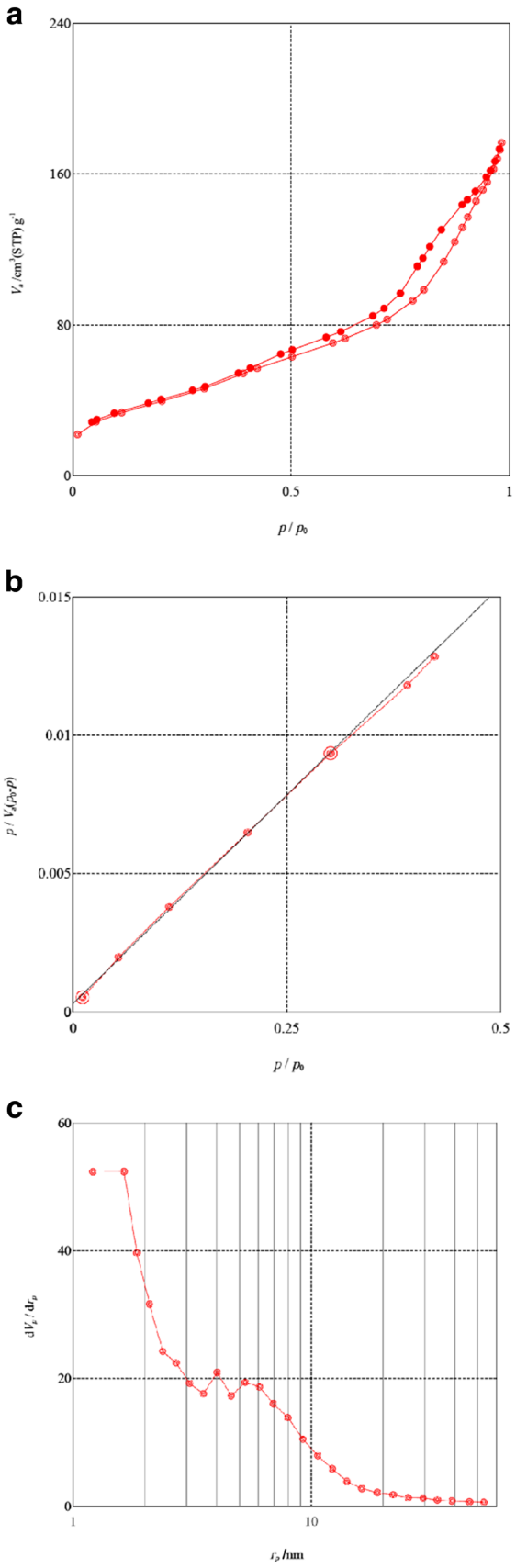

Fig. 8 **a** adsorption-desorption isotherms and **b** BET plot, **c** and BJH plot of Fe_3O_4@mSiO_2@GO nanoparticles

50–60 °C for 12 h. Finally the NPs are collected by magnet and are washed by methanol. The precipitation is dried at 40 °C for 2 h.

In the next step, commercial doxorubicin (2000 ppm) (1 mL) is diluted by water (1 mL). The attenuated drug (1000 ppm) and the naked DDS are blended with 10:1 mass proportion. This mixture is stirred by magnetic stirrer for 24 h at room temperature. Then polymeric shell (1 g) is introduced into the container and the mixture is stirred at room temperature for another 24 h. The loaded core-shell DDS is collected by magnet and is dried slowly at 4–6 °C for 48 h. The segregated solution of this mixture is used for measuring the amount of loaded drug.

Measuring of drug release in vitro

To measure drug release, powdered core-shell DDS (0.008 g) is ultrasonicated in PBS buffer (0.6 mL) for 7–10 s and then this colloidal solution is removed into a dialysis bag (12000 Dalton). This dialysis bag is then placed in a container with PBS buffer (5 mL). The surrounding solution of the bag is stirred by a magnetic stirrer of 270 rpm at 37 °C. The same procedure is applied to neutral buffer (pH=7.4). Accumulative drug release is measured in 1 h intervals by UV–Vis spectrophotometer at 480 nm. For the naked DDS the same method is used and the experimental condition is kept identical for all four experiments.

Results and discussion

Table 3 indicates the results of CHN analysis for GO and magnetized GO (Fe_3O_4@GO). Taking into account these results, they denote that for Fe_3O_4@GO we have this mass ratio:

$$\frac{\text{Fe3O4}}{\text{GO}} = \frac{79.54}{20.46}$$

This ratio states that almost 80 % of the mass of Fe_3O_4@GO is constituted of Fe_3O_4 NPs.

The wide angle XRD pattern shows an indicative peak of GO at around 12° [19]. By using the selection rules for Bravais lattices, the [220], [311], [400], [422], [511] and [440] sets confirm the fcc lattice structure of Fe_3O_4 NPs (Fig. 5). It is worthwhile to note that the characteristic peak of GO is absent in the XRD pattern of Fe_3O_4@GO. This is due

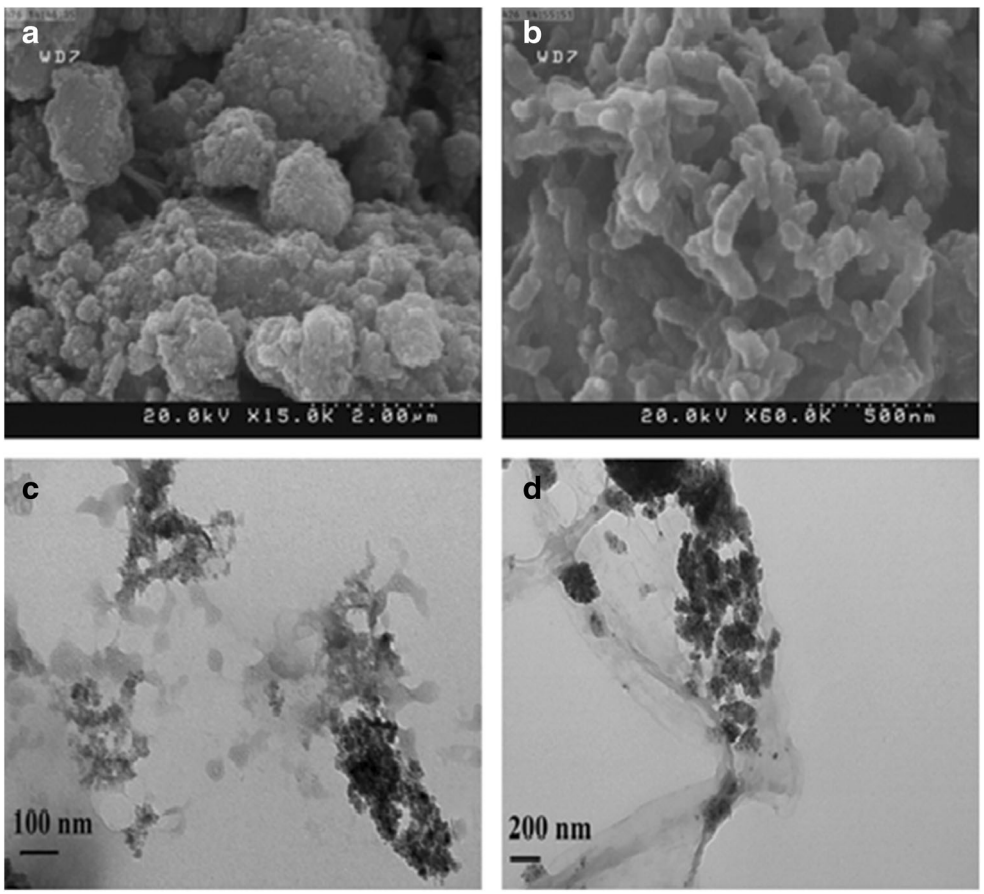

Fig. 9 SEM images of the naked DDS (**a**) and core-shell DDS (**b**) and TEM images of the naked DDS (**c**) and core-shell DDS (**d**)

to the structural distortion of GO nano-sheets that is brought about by Fe_3O_4 NPs [20]. The XRD pattern of magnetized mesoporous GO (Fe_3O_4@$mSiO_2$@GO) is the same as that of Fe_3O_4@ GO, due to the fact that the indicative peak of mesoporous NPs is detectable at $2\theta<4°$ [21, 22].

FT-IR spectrum of magnetized mesoporous GO (Fe_3O_4@$mSiO_2$@GO) approves the existence of expected NPs (Fig. 6a): two indicative peaks of bending and stretching vibration of (Fe-O) are detectable at 578.62 cm^{-1} and 632.60 cm^{-1}. The characteristic peak at 1046.59 cm^{-1} is assigned to the (Si-O-Si) stretching which is due to the existence of mesoporous NPs. The peaks at 1625.76 cm^{-1} and 3430.46 cm^{-1} are assigned to (H-O-H) bending and (O-H) stretching, arose from remnant water in mesoporous structure [23].

In the FT-IR spectrum of Fe_3O_4@$mSiO_2$@GO/acrylate, the characteristic band at 1731.43 cm^{-1} is assigned to the ester group (Fig. 6c). This band is absent in the naked DDS (Fe_3O_4@$mSiO_2$@GO/hexamine) spectrum because of binding of pentaethylene hexamine group into the carbonyl group. The band at 1305.98 cm^{-1} is assigned to (C-N) stretching and the one at 1566.08 cm^{-1} is assigned to (H-N-H) bending (Fig. 6b).

The FT-IR spectrum of mPEG-acrylate shows a strong peak at 1723.31 cm^{-1} which is assigned to ester group. Also the indicative peak of ether groups could be seen at 1112.84 cm^{-1} (Fig. 7a). The FT-IR spectrum of mPEG-acrylate-*g*-(alginate-co-poly acrylic acid) shows a weakened shoulder at 1728.41 cm^{-1} which is indicative of ester groups in the polymer structure. The peaks at 1036.56 and 1097.66 cm^{-1} are assigned to the ether groups. The peaks at 1417.69 and 2938.59 cm^{-1} are related to the stretching and overtone of C-H bond respectively (Fig. 7b).

Using adsorption and desorption BET isotherms of Fe_3O_4@$mSiO_2$@GO, physical properties of pores are calculable (Fig. 8). The total pore volume, surface area and the average pore diameter are 0.27 cm^3/g, 143 m^2/g and 7.7 nm respectively.

SEM image demonstrates the layered structure of GO nano-sheets with Fe_3O_4 NPs on it (Fig. 9a). From this image it can be inferred that the approximate size of an average GO nano-sheet is less than 2 μm. In the TEM image, the porous structure of the mesoporous NPs is quite apparent (Fig. 9c). From this image the pore diameter of mesoporous NPs is almost 8 nm which is in great accordance with BET results. The dark spots in this image are Fe_3O_4 NPs.

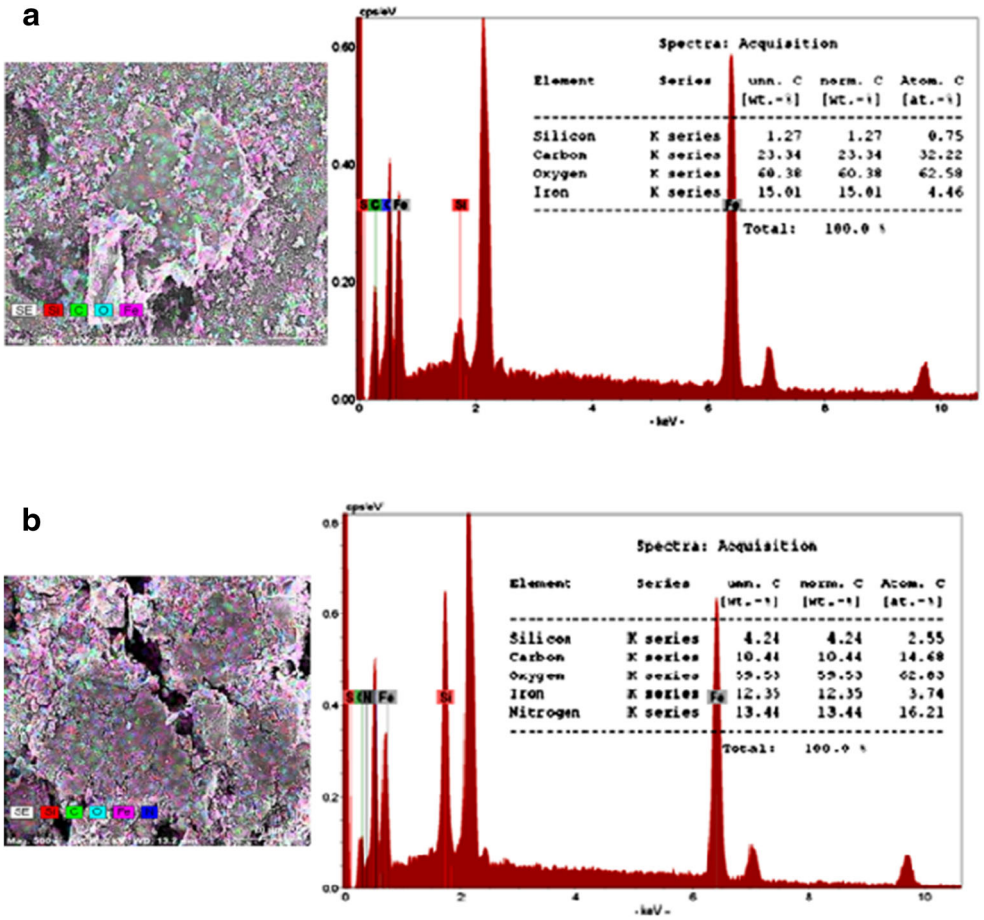

Fig. 10 EDX analysis images and results of **a** Fe_3O_4@$mSiO_2$@GO and **b** core-shell DDS

Figure 9b and d demonstrate the SEM and TEM images of the core-shell DDS. In these images the lamellar structure of GO nano-sheets and the fine structure of mesoporous NPs are not discernible because the polymeric shell has enveloped the core of the DDS; instead an entangled tubular network could be discerned which is indeed the polymeric skeleton.

The exact quantitative and qualitative characteristics of the constituents of NP are obtained by work function of the elements in EDX analysis. Figure 10a and b shows the mass percentage of the Fe_3O_4@$mSiO_2$@GO and core-shell DDS constituents, respectively. The existence of two indicative peaks for iron, confirms the entity of Fe(II) and Fe(III) in the inverse spinel structure of the Fe_3O_4 lattice.

The topographic features of Fe_3O_4@$mSiO_2$@GO were determined by AFM images. The specified width and height of an average Fe_3O_4 NP are 27.35 nm and 0.2946 nm respectively (Fig. 11a). Comparing the AFM image of the core-shell DDS with that of Fe_3O_4@$mSiO_2$@GO is worthwhile; while the width of the two chosen spots are relatively identical, the height of the chosen spot in the core-shell DDS (3.141 nm) is almost tenfold that of naked DDS (0.2946 nm) which in turn approves the existence of a polymeric shell (Fig. 11b).

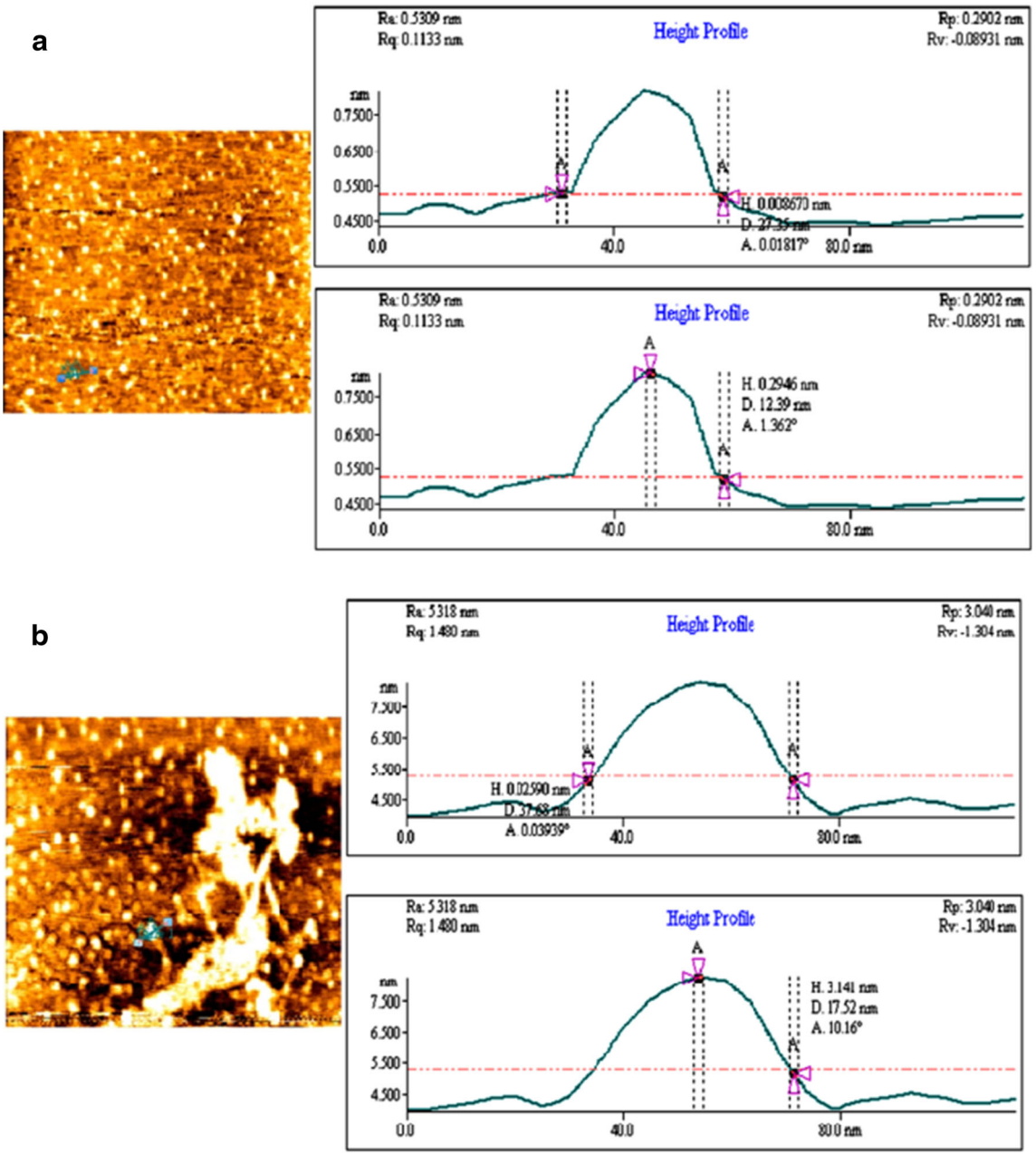

Fig. 11 AFM images and topographic diagrams of **a** Fe_3O_4@$mSiO_2$@GO and **b** core-shell DDS

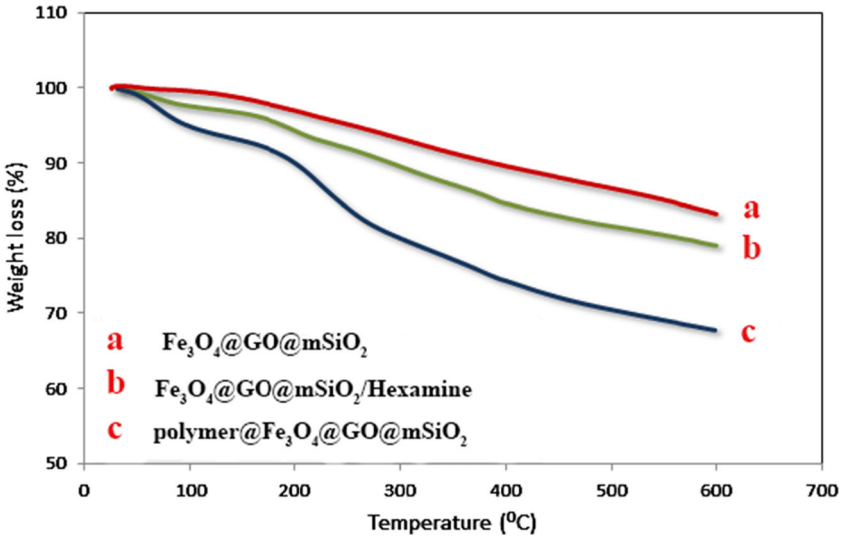

Fig. 12 Thermogravimetric analysis (TGA) results which determines the polymeric content of the NPs

Figure 12 shows the results of thermogravimetric analysis. The TGA diagram of Fe_3O_4@$mSiO_2$@GO shows 17 % weight loss owing to the oxidation of functional groups (carboxylic acid, hydroxyl etc.) and evaporation of the remnant water in the mesoporous structure. The TGA diagram of Fe_3O_4@$mSiO_2$@GO/hexamine shows 4 % weight loss more than Fe_3O_4@$mSiO_2$@GO. This is assigned to the oxidization of pentaethylene hexamine oligomers. The TGA diagram of core-shell DDS shows 11 % more weight loss in comparison with Fe_3O_4@$mSiO_2$@GO/hexamine which is totally ascribed to the polymeric shell.

The colloidal stability of the Fe_3O_4@$mSiO_2$@GO/hexamine was determined by zeta (ζ) potential analysis. The high measured potential (−20.7 mV) proves the stability of this NP in aqueous media. However the ζ potential of the core-shell DDS is even more than this (+45.1 mV),

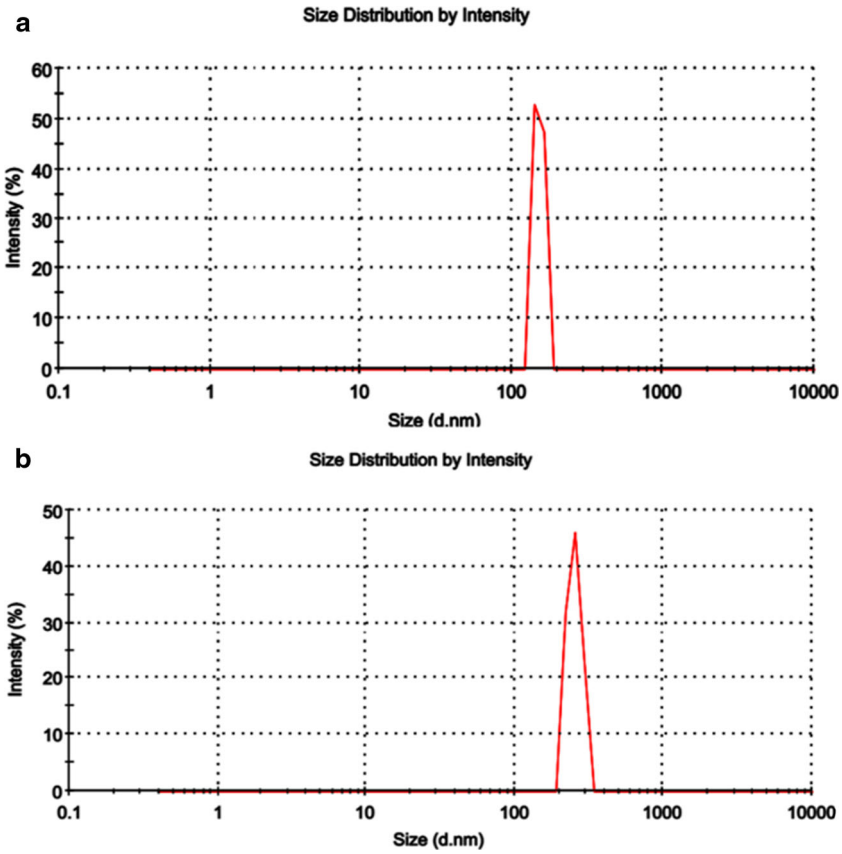

Fig. 13 DLS analysis results for **a** Fe_3O_4@$mSiO_2$@GO and **b** core-shell DDS

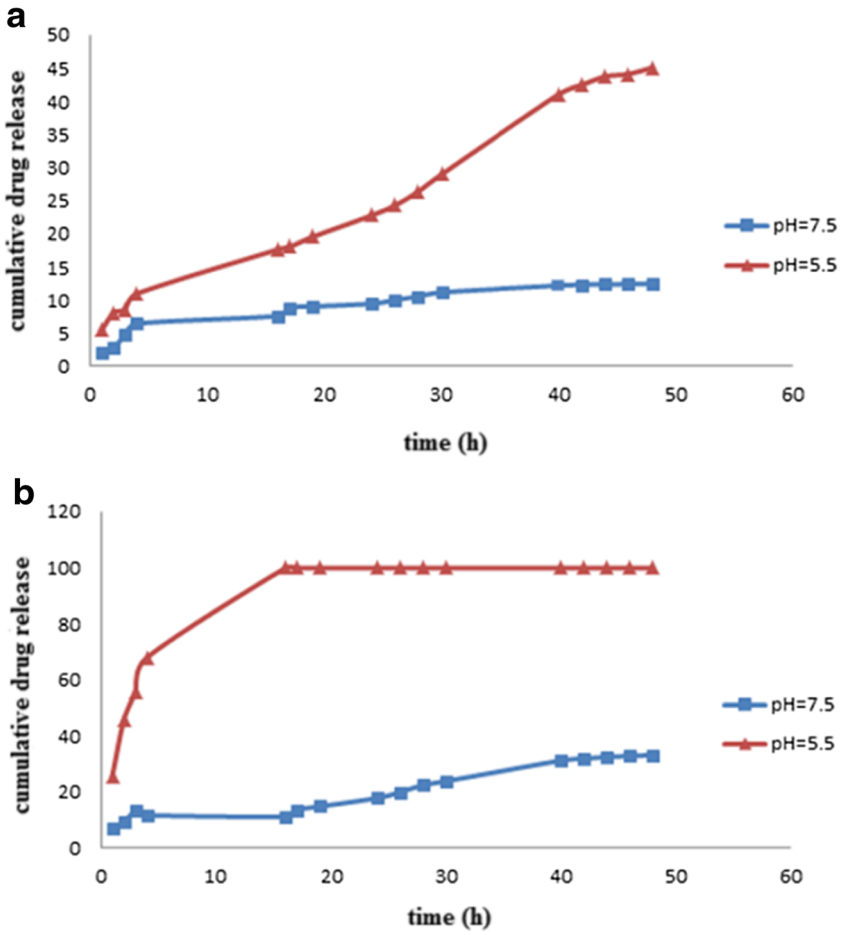

Fig. 14 cumulative drug release% of a core-shell DDS and **b** naked DDS in acidic and neutral media

which guarantees its high colloidal stability in biological medium.

The DLS analysis revealed the size of Fe_3O_4@mSiO_2@GO NP to be 152 nm with PdI=1.000 (Fig. 13a). The superficial discordance between the size determined by SEM image and the size determined by DLS analysis stems from differences in sample preparation. In the samples prepared for SEM, NPs are coagulated and the size of the NP is bigger than the actual size (152 nm). Furthermore the size of the core-shell DDS proved to be 253 nm (with PdI= 0.792) which seems to be an adequate size for a drug delivery system (Fig. 13b).

In vitro drug release

Figure 14a shows the results of in vitro drug release for the core-shell DDS. Equation (1) was used to calculate the cumulative drug release%. By far the core-shell DDS is sensitive to an acidic medium and releases more than 45 % of its drug load in the first 48 h, while in the same time span in a neutral medium it releases 10 % of its drug load. Figure 14b provides the results of the same experiment for the naked DDS. In an acidic medium this drug carrier liberates its whole drug content in less than 20 h whereas in a neutral medium a bit more than 30 % of the drug content is liberated. These results contrast the role of a polymeric shell in a sustainable drug release.

$$\text{Cumulative drug release}\% = \frac{W(freed\ drug)}{W(loaded\ drug)} \times 100 \quad (1)$$

Using Eqs. (2) and (3), the entrapment efficiency% and the loading content% are calculable for both core-shell DDS and the naked DDS (Table 4).

$$\text{Entrapment efficiency}\% = \frac{W(fed\ drug) - W(supernatant\ drug)}{W(fed\ drug)} \times 100 \quad (2)$$

Table 4 Loading content% and Entrapment efficiency% associated with two types of DDS

Type of the DDS	Loading content%	Entrapment efficiency%
Core-shell DDS	21	93.5
Naked DDS	10	82

$$\text{Loading content}\% = \frac{W(fed\ drug) - W(supernatant\ drug)}{W(loaded\ DDS)} \times 100 \quad (3)$$

Conclusion

This synthesis, though complicated, proposes a new DDS that has benefited from several renowned nanoparticles in the drug delivery realm. Its dual-targeting nanostructure is composed of magnetite nanoparticles, which could be led and concentrated via an external magnetic field, as well as a novel pH-sensitive oligomer which could be safer than its analogues utilized pH-sensitive moieties. In comparison with other similar carrier systems, the drug loading capacity of the DDS was increased by introducing mesoporous nanoparticles. To escalate the biocompatibility and immunocompatibility of DDS, PEG groups were attached to the shell of the drug carrier. The results of in vitro cumulative drug release not only prove the core-shell DDS as a practical and promising one but contrast and compare the role of a polymeric shell for the DDS. Based on the outcomes of this work, it can be concluded that the synthesized core-shell DDS is quite sensitive to the pH of tumor bearing tissue (pH=5.5) and can be utilized for improving the therapeutic efficacy of anticancer drugs and decreasing their side effects.

References

1. Eid M (2013) J Polym Res 112:1–11
2. Naahidi S, Jafari M, Edalat F, Raymond K, Khademhosseini A, Chen P (2013) J Control Release 166:182–194
3. Gillies RJ, Robey I, Gatenby RA (2008) J Nucl Med 49:24–42
4. Bartil T, Bounekhel M, Cedric C, Jerome R (2007) Acta Pharm 57: 301–314
5. Risbud MK, Hardikar AA, Bhat SV, Bhonde RR (2000) J Control Release 68:23–30
6. Gupta KC, Kumar MNVR (2000) Polym Int 49:141–146
7. Singh SK, Singh MK, Kulkarni PP, Sonkar VK, Grácio JJA, Dash D (2012) ACS Nano 6:2731–2740
8. Deshmukh K, Khatake SM, Joshi GM (2013) J Polym Res 286:1–11
9. Yang K, Zhang S, Zhang G, Sun X, Lee ST, Liu Z (2010) Nano Lett 10:3318–3323
10. Wang S (2009) Microporous Mesoporous Mater 117:1–9
11. Hartmann M (2005) Chem Mater 17:4577–4593
12. Yiu HHP, Wright PA (2005) J Mater Chem 15:3690–3700
13. Calero M, Gutierrez L, Salas G, Luengo Y, Lazaro A, Acedo P, Morales MP, Miranda R, Villanueva A (2014) Nanomed Nanotechnol Biol Med 10:733–743
14. Cornell RM, Schwertmann U (2003) The iron oxides: structure, properties, reactions, occurrences and uses; Wiley: Weinheim,; 2nd Edition, Chapter 1: 3–7
15. Lu XJ, Forssberg E (2002) Miner Eng 15:755–757
16. Marcano DC, Kosynkin DV, Berlin JM, Sinitskii A, Sun Z, Slesarev A, Alemany LB, Lu W, Tour JM (2010) ACS Nano 4: 4806–4814
17. Wang G, Yang S, Wei Z, Dong X, Wang H, Qi M (2013) Polym Bull 70:2359–2371
18. Yin P, Sun N, Deng C, Li Y, Zhang X, Yang P (2013) Proteomics 13:2243–2250
19. Long D, Li W, Ling L, Miyawaki J, Mochida I, Yoon SH (2010) Langmuir 26:16096–16102
20. Han Q, Wang Z, Xia J, Chen S, Zhang X, Ding M (2012) Talanta 101:388–395
21. Gusev VY, Feng X, Bu Z, Haller GL, O'Brien JA (1996) J Phys Chem 100:1985–1988
22. Zhao D, Huo Q, Feng J, Chmelka BF, Stucky GD (1998) J Am Chem Soc 120:6024–6036
23. Coates J (2000) Interpretation of infrared spectra, a practical approach. Wiley: Chichester: 10815–10837